HAL
open science

Helicobacter pylori UreE, a urease accessory protein: specific Ni2+ and Zn2+ binding properties and interaction with its cognate UreG

Matteo Bellucci, Barbara Zambelli, Francesco Musiani, Paola Turano, Stefano Ciurli

To cite this version:

Matteo Bellucci, Barbara Zambelli, Francesco Musiani, Paola Turano, Stefano Ciurli. Helicobacter pylori UreE, a urease accessory protein: specific Ni2+ and Zn2+ binding properties and interaction with its cognate UreG. Biochemical Journal, 2009, 422 (1), pp.91-100. 10.1042/BJ20090434 . hal-00479178

HAL Id: hal-00479178

https://hal.science/hal-00479178v1

Submitted on 30 Apr 2010

HAL is a multi-disciplinary open access archive for the deposit and dissemination of scientific research documents, whether they are published or not. The documents may come from teaching and research institutions in France or abroad, or from public or private research centers.

L'archive ouverte pluridisciplinaire **HAL**, est destinée au dépôt et à la diffusion de documents scientifiques de niveau recherche, publiés ou non, émanant des établissements d'enseignement et de recherche français ou étrangers, des laboratoires publics ou privés.

Biochemical Journal Immediate Publication. Published on 29 May 2009 as manuscript BJ20090434

Helicobacter pylori UreE, a urease accessory protein: specific Ni^{2+} and Zn^{2+} binding properties and interaction with its cognate UreG

Matteo Bellucci[*], Barbara Zambelli,[*] Francesco Musiani,[*] Paola Turano,[†] and Stefano Ciurli[*,†]

[*]Laboratory of Bioinorganic Chemistry, Department of Agro-Environmental Science and Technology, University of Bologna, Via Giuseppe Fanin 40, I-40127 Bologna (Italy) and [†]CERM (Centre for Magnetic Resonance), University of Florence, Via Luigi Sacconi 6, I-50019 Sesto Fiorentino (Italy)

The persistence of *Helicobacter pylori* in the hostile environment of the human stomach is ensured by the activity of urease. The essentiality of Ni^{2+} for this enzyme demands proper intracellular trafficking of this metal ion. The metallo-chaperone UreE promotes Ni^{2+} insertion into the apo-enzyme in the last step of urease maturation while facilitating concomitant GTP hydrolysis. This study focuses on the metal-binding properties of UreE from *Helicobacter pylori* (*Hp*UreE) and its interaction with the related accessory protein *Hp*UreG, a GTPase involved in the assembly of the urease active site. Isothermal titration calorimetry (ITC) showed that *Hp*UreE binds one equivalent of Ni^{2+} (K_d = 0.15 μM) or Zn^{2+} (K_d = 0.49 μM) per dimer, without modification of the protein oligomeric state, as indicated by light scattering. Different ligand environments for Zn^{2+} and Ni^{2+}, which involve crucial histidine residues, were revealed by site-directed mutagenesis, suggesting a mechanism for discriminating metal ion specific binding. The formation of a *Hp*UreE-*Hp*UreG protein complex was revealed by NMR spectroscopy, and the thermodynamics of this interaction were established using ITC. A role for Zn^{2+}, and not for Ni^{2+}, in the stabilization of this complex was demonstrated using size exclusion chromatography, light scattering, and ITC experiments. A calculated viable structure for the complex suggested the presence of a novel binding site for Zn^{2+}, actually detected using ITC and site-directed mutagenesis. The results are discussed in relation to available evidences of a UreE-UreG functional interaction in vivo. A possible role for Zn^{2+} in the Ni^{2+}-dependent urease system is envisaged.

Key words: *Helicobacter pylori* urease assembly, nickel trafficking, zinc binding, accessory protein UreE, accessory protein UreG, protein-protein complex formation

Address for correspondence: Prof. Stefano Ciurli, Laboratory of Bioinorganic Chemistry, Department of Agro-Environmental Science and Technology, University of Bologna (Italy), Viale Giuseppe Fanin 40, I-40127 Bologna (Italy); Phone: +39-051-209-6204; FAX: +39-051-209-6203; email: stefano.ciurli@unibo.it

Running title: *Helicobacter pylori* UreE, metal ions and UreG

Abbreviations: *Hp*: *Helicobacter pylori*; *Bp*: *Bacillus pasteurii*; *Ka*: *Klebsiella aerogenes*; *Mj*: *Methanocaldococcus jannaschii*; CD: circular dichroism; ITC: isothermal titration calorimetry; SEC: size exclusion chromatography; MALS: multiple angle light scattering; QELS: quasi-elastic light scattering; NMR: nuclear magnetic resonance spectroscopy; TROSY: transverse relaxation optimized spectroscopy; HSQC: heteronuclear single quantum correlation; NRMSD: normalized root mean square deviation.

THIS IS NOT THE VERSION OF RECORD - see doi:10.1042/BJ20090434

Accepted Manuscript

Licenced copy. Copying is not permitted, except with prior permission and as allowed by law.
© 2009 The Authors Journal compilation © 2009 Portland Press Limited

THIS IS NOT THE VERSION OF RECORD - see doi:10.1042/BJ20090434

INTRODUCTION

Helicobacter pylori is a widespread human pathogen that colonizes the gastric mucosa of ca. 50% of the world human population [1] and is responsible for severe diseases such as chronic gastritis, peptic and duodenal ulcers that eventually may lead to cancer [2]. The bacterium is able to survive in the hostile environment of the human stomach through the activity of urease. This enzyme catalyzes the hydrolysis of urea to ultimately yield ammonium and bicarbonate ions, thus causing an increase of the acidic local pH of the mucosa to values compatible with the survival of this pathogen. The remarkable enhancement of the rate of the reaction catalyzed by urease as compared to the uncatalyzed reaction (3 x 10^{15} fold) [3] is determined by the unique presence, among hydrolases, of Ni^{2+} ions in the active site of the enzyme [4]. Several crystal structures of urease from bacteria [5-7] and plants [8] are available. The active site of the enzyme contains two essential Ni^{2+} ions bridged by a fully conserved, post-translationally carbamylated, lysine residue, and by a hydroxide ion, which acts as the nucleophile in the catalytic mechanism [9].

In general, the essentiality of Ni^{2+} for the activity of urease, together with the intrinsic cellular toxicity of this metal ion, requires a proper intracellular Ni^{2+} handling. In particular, urease is assembled in vivo as an inactive apo-enzyme, and undergoes a maturation process that involves Ni^{2+} incorporation and lysine carbamylation to produce a fully active holo-enzyme [10]. This assembly process requires the involvement of dedicated accessory proteins, namely UreD (UreH in *H. pylori*), UreF, UreG, and UreE. The current model for this process [10] entails the formation of a protein complex between the apo-enzyme and these protein chaperones, followed by the delivery of Ni^{2+} concomitantly with the GTP-dependent transfer of a CO_2 molecule necessary for lysine carbamylation. Among all urease accessory proteins, the structural properties and role of UreD remain largely obscure: this protein has been proposed to bind to apo-urease, thus inducing a conformational change required for the subsequent steps of the activation process [11], an hypothesis recently supported by small angle X-ray scattering results [12]. The latter study also appears to indicate that UreF contributes to this conformational change, which ultimately allows CO_2 and Ni^{2+} ions to gain access to the nascent active site. UreG is responsible for the GTP hydrolysis associated to the transfer of CO_2 to the active site lysine: the protein is intrinsically disordered, specifically binds Zn^{2+}, and features very low or absent hydrolyzing activity in vitro, probably needing the interaction with other protein partners to achieve its fully folded and functional structure [13-16]. UreF has been proposed to act as an activator of the GTPase activity of UreG on the basis of structural bio-modelling studies [17].

UreE is believed to act as a Ni^{2+} carrier based on the evidence that the levels of Ni^{2+} necessary for the in vitro assembly of the urease active site are significantly reduced, and a much larger portion of enzyme molecules is activated, if UreE is present [11, 18, 19]. The crystal structures of *Bacillus pasteurii* UreE (*Bp*UreE [20]) and of a truncated form of *Klebsiella aerogenes* UreE (H144**Ka*UreE [21]), indicate that UreE are symmetric homodimers, with each monomer made of an N-terminal domain and a C-terminal domain, the latter involved in the head-to-head dimerization. A metal ion binding site, found at the protein dimerization interface, involves two conserved histidines, one from each monomer (His^{100} in *Bp*UreE and His^{96} in *Ka*UreE, Figure 1A). This site contains Zn^{2+} in the structure of *Bp*UreE and Cu^{2+} in that of H144**Ka*UreE, but is generally assumed to be occupied by Ni^{2+} in the protein functional form in vivo, an hypothesis supported by anomalous difference X-ray diffraction maps of *Bp*UreE crystals soaked in a Ni^{2+} solution [20]. The structure of H144**Ka*UreE also contains two additional Cu^{2+} ions, bound to a pair of histidines on the surface of each monomer (His^{110}, His^{112}), but these residues are not conserved in *Bp*UreE (Tyr^{114}, Lys^{116}), *Hp*UreE (Phe^{118}, Lys^{120}) (Figure 1) and other sources [22].

An alternative possible physiological role for UreE is suggested by the observation that the GTP concentration needed for optimal activation of urease in vitro is greatly reduced in the presence of UreE as compared to that required in its absence [19]. This implies that UreE must play an important direct or indirect role in the functional activation of UreG. In this respect, in vivo studies using yeast two-hybrid analysis [23, 24] as well as co-immunoprecipitation assays [24] indicated a direct interaction between UreE and UreG from *Helicobacter pylori*.

On the basis of the available evidence, the question of which functional role is played by UreE in the urease active site assembly is still awaiting a definitive answer. The present study represents an

Licenced copy. Copying is not permitted, except with prior permission and as allowed by law.
© 2009 The Authors Journal compilation © 2009 Portland Press Limited

attempt to clarify some details of the reactivity of UreE towards Ni^{2+} and Zn^{2+}, as well as with *Hp*UreG.

Figure 1 here

EXPERIMENTAL

Protein preparations

Recombinant wild type *Hp*UreE was prepared using a protocol adapted from an earlier report [25]. Purity was checked using SDS-PAGE (see Figure S1, in Supplementary Information). Site-directed mutagenesis, aimed at the production of the H102K and H152A mutants, was carried out using standard procedures. The full experimental details of gene cloning, protein expression and purification are provided as Supplementary Information. Recombinant *Hp*UreG and its C66A/H68G mutant were obtained as previously described [16].

Circular dichroism spectroscopy

The secondary structure of *Hp*UreE was evaluated by circular dichroism spectroscopy, performed on the protein (5 μM) diluted in 20 mM phosphate buffer, pH 8.0, using a JASCO 810 spectropolarimeter flushed with N_2, and a cuvette with 0.1 cm path-length. Ten spectra were accumulated from 190 to 240 nm at 0.2 nm intervals, and averaged to achieve an appropriate signal-to-noise ratio. The spectrum of the buffer was subtracted. The secondary structure composition of *Hp*UreE was evaluated using the CDSSTR tool available on the Dichroweb server, with the reference sets 3, 4, 6, and 7 (http://www.cryst.bbk.ac.uk/cdweb/html/home.html).

NMR spectroscopy experiments

Uniformly ^{15}N-labeled *Hp*UreE and *Hp*UreG were produced with the same purification procedure used for the unlabeled proteins, using M9 minimal medium containing $^{15}NH_4Cl$ as sole nitrogen source. Solutions containing ^{15}N-labeled *Hp*UreE (200 μM) and unlabeled *Hp*UreG, or ^{15}N-labeled *Hp*UreG (300 μM) and unlabeled *Hp*UreE, were prepared mixing one equivalent of the *Hp*UreE dimer with two equivalents of the *Hp*UreG monomer. ^{1}H-^{15}N heteronuclear single quantum correlation (HSQC) experiments [26] and transverse relaxation optimized spectroscopy (TROSY)-HSQC experiments [27] were carried out at 298 K on a Bruker 800 MHz spectrometer equipped with a TXI cryoprobe. The acquisition parameters for these NMR spectra are provided as Supporting Information (Table S1). Spectra were processed and analyzed using TopSpin (Bruker) and iNMR (http://www.inmr.net/).

Light scattering measurements

In a typical experiment, a protein sample (100 μL, 50 μM) was loaded onto a size-exclusion Superdex 200 HR 10/30 column (GE Healthcare), pre-equilibrated using 20 mM TrisHCl, pH 8.0, 150 mM NaCl, and eluted at a flow rate of 0.6 mL min^{-1}. The column was connected downstream to a multi-angle laser light (690.0 nm) scattering DAWN EOS photometer (Wyatt Technology) and to a quasi-elastic light scattering WyattQELS device. The concentration of the eluted protein was determined using a refractive index detector (Optilab DSP, Wyatt). The specific refractive index increment (dn/dc) for the proteins was taken as 0.185 mL/g [28]. The value of 1.321 was used for the solvent refractive index. Molecular weights were determined from a Zimm plot. Data were recorded and processed using the Astra 5.1.9 software (Wyatt Technology), following the manufacturer's indications. When the measurements were carried out in the presence of metal ions, stoichiometric amounts of $ZnSO_4$ or $NiSO_4$ were added to the protein samples before loading it onto the size-exclusion column, and the protein was eluted using the same buffer containing 20 μM $ZnSO_4$ or $NiSO_4$. In order to explore the formation of a *Hp*UreE-*Hp*UreG interaction, a solution containing *Hp*UreE (50 μM dimer) and *Hp*UreG (100 μM monomer) was analyzed in the absence and in the presence of 200 μM $NiSO_4$ or 200 μM $ZnSO_4$ under the same experimental conditions.

Isothermal titration calorimetry experiments

Titration experiments were performed at 25 °C using a high-sensitivity VP-ITC microcalorimeter (MicroCal LLC, Northampton, MA). The proteins and the metal ions (from 100 mM stock solutions) were diluted using the same buffer (20 mM TrisHCl, pH 7.0, 150 mM NaCl) eluted from a size exclusion column utilized immediately before the ITC measurement to freshly purify the protein. The measuring cell contained 1.4093 mL of protein solution, and the reference cell was filled with

THIS IS NOT THE VERSION OF RECORD - see doi:10.1042/BJ20090434

Accepted Manuscript

Licenced copy. Copying is not permitted, except with prior permission and as allowed by law.
© 2009 The Authors Journal compilation © 2009 Portland Press Limited

THIS IS NOT THE VERSION OF RECORD - see doi:10.1042/BJ20090434

deionized water. Before starting the experiments, the baseline stability was verified. A spacing of 400-600 s between injections was applied in order to allow the system to reach thermal equilibrium after each addition. For each titration, a control experiment was carried out by adding the titrating solution into the buffer alone, under identical conditions. Heats of dilution were negligible. In a set of experiments aimed at determining the metal binding properties of *Hp*UreE, the protein (10 μM) or its H102K and H152A mutants (10 μM) were titrated with 30 injections (10 μL each) of a solution containing 100 μM $NiSO_4$ or $ZnSO_4$. In order to determine the binding parameters of *Hp*UreE to *Hp*UreG, the latter protein (50 μM monomer) was titrated with 30 injections (10 μL each) of a solution containing 160 μM *Hp*UreE dimer in the same buffer. In the case of Zn^{2+} titration onto the *Hp*UreE-*Hp*UreG complex (5 μM) generated in situ by mixing 5 μM *Hp*UreE and 10 μM *Hp*UreG monomer, 30 aliquots (10 μL each) of a solution containing 70 μM $ZnSO_4$ were injected into the protein solution. Identical set up was used for the related mutants. The details of data analysis are given as Supplementary Information. The dissociation constants and thermodynamic parameters provided in the article do not take into account possible events of proton transfer linked to metal binding, or the presence, in solution, of complexes between the metal ions and the buffer. This treatment is beyond the scope of the present study. However, the values of the measured equilibrium constants compare well with those reported in the literature and determined using ITC or other methodologies such as equilibrium dialysis coupled to metal analysis, which, in principle, should also take into account similar effects. These values are therefore only used for comparison purposes.

Structural modelling of the HpUreE-HpUreG complex

The alignment of *Bp*UreE and *Hp*UreE [22] was used to calculate, using the MODELLER9v5 software [29], 50 structural models of the *Hp*UreE dimer, imposing the structural identity of the two monomers. The best model was selected on the basis of the lowest value of the MODELLER objective function. The ROSETTADOCK software [30] was used to calculate an initial complex between the model structure of dimeric *Hp*UreG [16], and the central C-terminal domains of dimeric *Hp*UreE. The complex with the best ROSETTADOCK score was selected among all generated models for the subsequent refining run, carried out by applying 1000 times a perturbation to the starting structure. The Cα trace of this complex was used, together with the crystal structures of *Methanocaldococcus jannaschiii* (*Mj*HypB [31], PDB code 1HF8), *Bp*UreE [20] (PDB code 1EAR), and *Ka*UreE [21] (PDB code 1GMW) as templates to build 200 structural models of the *Hp*UreE - *Hp*UreG complex using the MODELLER9v5 software [29]. The best model was selected on the basis of the lowest value of the MODELLER objective function. The full details of the model calculation are provided as Supplementary Information.

RESULTS AND DISCUSSION

*Hp*UreE structural properties

A prediction of the secondary structure elements of *Hp*UreE (Figure 1B) based on the JPRED algorithm [32] indicates 21% α-helix and 23% β-strand content, with the remaining 56% constituting turns or random coil conformations. Figure 1B also suggests that a similar fold is attained by several different UreE proteins, as previously proposed on the basis of modelling studies [22]. The CD spectrum of *Hp*UreE (Figure 2A) shows the presence of both α-helices and β-strands, with negative deflections around 218 nm and 208 nm and a positive peak at 190 nm. The CD spectrum was quantitatively analyzed and the best fit (NRMSD = 0.029) estimated a secondary structure composition of 13% α-helix, 33% β-strand, 23% turns and 30% random coil for *Hp*UreE. This composition is similar to that calculated using the DSSP program [33] for the crystallographic structures of Zn^{2+}-bound *Bp*UreE [20] (18% α-helix, 37% β-sheet) and of the Cu^{2+}-bound H144*KaUreE [21] (13% α-helix, 25% β-sheet). The ^{1}H chemical shift spreading observed in the TROSY-HSQC NMR spectrum (Figure 2B) ranges from 6.5 to 10 ppm, as observed in the ^{1}H-^{15}N HSQC NMR spectrum of *Bp*UreE [34], suggesting similar extent of fold for the two proteins.

The molecular mass and the hydrodynamic radius of *Hp*UreE in solution were determined using a combination of size exclusion chromatography and light scattering (MALS/QELS) (Figure 2C). The elution profile and the light scattering data show that *Hp*UreE is a dimer in solution with M = 43.1 ± 4.8 kDa and R_h = 3.0 ± 1.4 nm (theoretical mass = 39 kDa). This is consistent with all available

Licenced copy. Copying is not permitted, except with prior permission and as allowed by law.
© 2009 The Authors Journal compilation © 2009 Portland Press Limited

crystallographic structural information on UreE proteins (Figure 1B) [20, 21] as well as with previous evidence collected on *Hp*UreE based on size-exclusion chromatography criteria [25]. The light scattering measurements exclude the possibility that oligomers of the apo-protein are formed in solution for concentrations lower than 50 μM, as instead previously proposed for H144**Ka*UreE [35]. The better quality of the ^{1}H-^{15}N TROSY-HSQC (Figure 2B) with respect to the simple ^{1}H-^{15}N HSQC experiment (data not shown) further supports the presence of a dimeric form at 0.1-0.3 mM concentration. The symmetric architectural arrangement of the two monomers is revealed by the number of observed peptide NH peaks in the NMR spectrum: about 120 unique peaks, out of the expected 170 residues per monomer, can be observed, with missing signals likely including the C-terminal 30 residues predicted to be unstructured using JPRED (Figure 1B). In particular, in the case of glycine residues, seven Gly are present in the sequence of *Hp*UreE (Figure 1B) and the same number of peaks is observed in the ^{15}N 100-110 ppm range typical for Gly NH signals (Figure 2B).

Figure 2 here

_Hp_UreE metal binding properties

Ni^{2+} is generally considered to be the physiological cofactor of UreE, and the understanding of the structural features of Ni^{2+} binding is therefore important to clarify the role of this chaperone in vivo. Moreover, in several recent instances, interplay between Ni^{2+} and Zn^{2+} has been observed and proposed to be functionally important in regulating cellular trafficking of metal ions [13-16, 31, 36-40]. In particular, Zn^{2+} is involved in the dimerization of *Hp*UreG, a process that plays a potential regulatory role in the urease active site assembly [16]. Previous equilibrium dialysis experiments carried out on *Hp*UreE established a 1:1 stoichiometry for the Ni^{2+} binding to the homodimeric protein, with K_d ca. 1 μM [25]. However, the experiments were carried out at pH 8.25 in an apparently non-buffered solution containing only NaCl, no thermodynamic parameters for the metal binding event were determined, nor the binding affinity for Zn^{2+} was measured [25]. In the present study, the Ni^{2+} binding to *Hp*UreE was investigated using isothermal titration calorimetry (ITC), and a comparison between Ni^{2+} and Zn^{2+} binding was performed.

The ITC measurements were carried out by adding Ni^{2+} or Zn^{2+} to the apo-protein in a buffered solution at pH 7.0, and the occurrence of a binding event was revealed by the presence of exothermic peaks that followed each addition (Figure S2A and S2B for Ni^{2+} and Zn^{2+}, respectively). Fits of the integrated heat data (Figure 3A and 3B for Ni^{2+} and Zn^{2+}, respectively) were carried out using the simplest model, which entails a single binding event, and yielded a stoichiometry of one equivalent of Ni^{2+} or Zn^{2+} bound to the *Hp*UreE dimer. Dissociation constants $K_d(Ni) = 0.15 \pm 0.01$ μM and $K_d(Zn) = 0.49 \pm 0.01$ μM were calculated for Ni^{2+} and Zn^{2+} binding, respectively. In both cases, these processes are driven by favourable enthalpic factors ($\Delta H(Ni) = -13 \pm 1$ kcal mol^{-1}, $\Delta H(Zn) = -10 \pm 1$ kcal mol^{-1}) that compensate the negative entropic values ($\Delta S(Ni) = -13$ cal mol^{-1} K^{-1}, $\Delta S(Zn) = -4$ cal mol^{-1} K^{-1}) calculated from the fit. The values of the $K_d(Ni)$ and $K_d(Zn)$ measured for *Hp*UreE are comparable to those established by ITC for the binding of Ni^{2+} and Zn^{2+} to *Bp*UreE and H144**Ka*UreE [35], and by equilibrium dialysis for the binding of Ni^{2+} to *Bp*UreE [39], of Ni^{2+} and Zn^{2+} to H144**Ka*UreE [41, 42] and of Ni^{2+} to *Hp*UreE [25]. All these values are consistent with a role of intracellular metal ion transport associated with UreE proteins [43].

Figure 3 here

In the structure of Zn^{2+}-*Bp*UreE [20] and Cu^{2+}-H144**Ka*UreE [21] the metal ions are bound to the surface of the protein using the conserved His^{100} and His^{96} residues, respectively (Figure 1A). In order to firmly establish the role of the corresponding His^{102} in the binding of Ni^{2+} and Zn^{2+} to *Hp*UreE, the H102K mutant was obtained by site-directed mutagenesis. ITC titrations of H102K *Hp*UreE with Ni^{2+} and Zn^{2+}, performed under identical conditions as for the wild type protein, proved the absence of a binding event (Figure 3A,B), confirming the key role of this residue in metal binding to *Hp*UreE.

In the crystal structure of Zn^{2+}-bound *Bp*UreE, the protein is present as a dimer of dimers, with

THIS IS NOT THE VERSION OF RECORD - see doi:10.1042/BJ20090434

Accepted Manuscript

Licenced copy. Copying is not permitted, except with prior permission and as allowed by law.
© 2009 The Authors Journal compilation © 2009 Portland Press Limited

the metal ion in a bridging position, bound to four conserved His[100] residues, one from each monomer [20]. However, this oligomerization has been observed for *Bp*UreE only in the solid state [20] or in concentrated (mM) solutions [34], while dynamic light scattering of the metal-bound protein in the 50-250 μM range excluded this effect [39].[1] In the case of *Hp*UreE, the influence of metal binding on the quaternary structure of the protein in the range of concentrations used in the microcalorimetric metal binding studies (10-20 μM) was investigated using a combination of light scattering methods (MALS and QELS). The values measured for Ni^{2+}-*Hp*UreE (M = 45.7 ± 5.1 kDa, R_h = 3.4 ± 1.5 nm) and Zn^{2+}-*Hp*UreE (M = 46.4 ± 5.2 kDa, R_h = 3.3 ± 1.5 nm) are similar to those established for the apo-protein (Figure 2C), demonstrating that the metal-bound protein is a dimer, and not a dimer of dimers, independently of the presence of bound metal ions. This is consistent also with the similar linewidths in the TROSY-HSQC NMR spectra of apo-, Ni^{2+}-bound and Zn^{2+}-bound *Hp*UreE, which indicates similar protein size in the various metal-bound states (Figure S3).

While the dissociation constants observed for the metal ion complexes of *Hp*UreE are in the μM range previously determined for UreE proteins from different sources, the 1:1 metal ion binding stoichiometry established for *Hp*UreE differs from previous data obtained for *Ka*UreE and *Bp*UreE, which indicated a 2:1 stoichiometry. *Ka*UreE additionally binds three Ni^{2+} ions to a His-rich tail containing 10 histidines among the last fifteen residues, absent both in *Hp*UreE and in *Bp*UreE [35]. In the case of *Bp*UreE, the presence of a binuclear $[Ni(OH)Ni]^{3+}$ centre was proposed on the basis of EXAFS spectra, rendering this protein not only a Ni^{2+} transporter but also a potential scaffold for the assembly of the dinuclear active site of urease [39]. In *Bp*UreE and *Ka*UreE a conserved HXH motif is present in this protein region: in particular, in *Bp*UreE the HQH motif is located at the end of the sequence, while in *Ka*UreE several possible HXH concatenated motifs constitute the His-rich tail (HGHHHAHHDHHAHSH). On the other hand, in *Hp*UreE a single histidine (His[152]) is observed in the C-terminal tail (Figure 1B). On the basis of these considerations, a possible reason for the different stoichiometry of the Ni^{2+} binding to *Hp*UreE on one side (1:1), and to *Bp*UreE and *Ka*UreE on the other (2:1), might reside in the different sequence motifs of histidine residues found at the C-terminal tails of these proteins. These observations suggest a specialized role, in metal ion storage and/or delivery, for the C-terminal portion of the protein, depending on its length and composition, and prompted us to investigate whether His[152] is involved in metal ion binding to *Hp*UreE using the H152A mutant.

ITC titrations of H152A *Hp*UreE with Ni^{2+}, performed under identical conditions as for the wild type protein, proved the occurrence of a binding event (Figure S2C). The integrated heat data, fitted using a single site model (Figure 3C), yielded values for the dissociation constant (K_d(Ni) = 0.87 ± 0.01 μM), reaction enthalpy (ΔH(Ni) = -12 ± 1 kcal mol^{-1}) and reaction entropy (ΔS(Ni) = -11 cal mol^{-1} K^{-1}) that are consistent with those obtained for the wild-type protein (Figure 3A). These data indicate that the His[152] residue is not involved in binding the Ni^{2+} ion in *Hp*UreE, suggesting that this residue is not essential for the nickel-delivery function. In turn, this also supports the concept that both histidine residues found in the HXH motif at the C-terminal end of *Bp*UreE and *Ka*UreE are necessary to build up the dinuclear Ni^{2+} centre observed in those cases.

On the other hand, the titration of H152A *Hp*UreE with Zn^{2+} showed clear differences in the binding mode as compared to the wild-type protein (Figure 3D and S2D). Best fits of the integrated heat data could be obtained using a model involving not one, as in the case of wild-type *Hp*UreE, but two independent binding events, yielding dissociation constants K_{d1}(Zn) = 0.13 ± 0.02 μM and K_{d2}(Zn) = 0.82 ± 0.01 μM. Both events are driven by favourable enthalpic (ΔH_1(Zn) = -4 ± 1 kcal mol^{-1}, ΔH_2(Zn) = -7 ± 1 kcal mol^{-1}) and entropic (ΔS_1(Zn) = 19 cal mol^{-1} K^{-1}, ΔS_2(Zn) = 6 cal mol^{-1} K^{-1}) factors. The observation of an additional Zn^{2+} binding site upon replacement of a histidine with a non-coordinating residue like alanine, could be, at first sight, bewildering. This apparent incongruity, resulting from our experimental data, can be explained by taking into consideration the peculiarity of the protein region where the mutation is carried out. This is a long

[1] The molecular mass and hydrodynamic radius of *Bp*UreE (50 μM dimer) in the absence and in the presence of two equivalents of Ni^{2+} and Zn^{2+} per dimer were determined in the present study using size exclusion chromatography on-line with MALS and QELS. The results indicate that, like *Hp*UreE, *Bp*UreE is a dimer in solution both in the absence and in the presence of these metals ions, with M = 41.0 kDa and R_h= 3.0 nm.

THIS IS NOT THE VERSION OF RECORD - see doi:10.1042/BJ20090434

Accepted Manuscript

Licenced copy. Copying is not permitted, except with prior permission and as allowed by law.
© 2009 The Authors Journal compilation © 2009 Portland Press Limited

extended and flexible stretch whose conformation or relative orientation with respect to the rest of the protein could change as a consequence of point mutations. Therefore, it is possible that, while His^{152} is involved in Zn^{2+} binding by isolated wild type *Hp*UreE, the resulting conformation of the flexible C-terminal arm masks an additional binding site, which becomes accessible upon mutation of this residue.

The conclusions that can be drawn from these results are that Ni^{2+} and Zn^{2+} bind to wild-type *Hp*UreE using different modes. While Ni^{2+} is bound to the conserved His^{102} on the surface of the dimer, without any involvement of His^{152}, Zn^{2+} binding not only requires the His^{102} pair, but is also modulated by the two His^{152} residues at the C-terminal position. A different binding mode for the two metal ions to the wild type protein is supported by a comparison of the TROSY-HSQC spectra of *Hp*UreE in the apo-form with the same spectra of the Zn^{2+} and Ni^{2+} bound forms (see Figure S3). Residues changing their chemical shifts upon nickel addition are also affected (and at the same extent) by the presence of zinc. In addition, a few more peaks change their position in the presence of Zn^{2+}, consistently with the involvement of a larger number of residues in the zinc-binding event. The higher availability of intracellular Zn^{2+} as compared to Ni^{2+}, together with the similar affinity of *Hp*UreE for these two metal ions described above, suggests that the specificity of binding different metals must rely on changes in ligand environment, as indeed observed experimentally.

At least one histidine residue is always present near the C-termini of all UreE sequences [22], while this feature is not maintained in the H152A *Hp*UreE mutant, nor in H144**Ka*UreE (Figure 1B). Consistently with this observation, the calorimetric Zn^{2+} titration curve obtained for H152A *Hp*UreE resembles the one reported for the binding of Ni^{2+} and Cu^{2+} to H144**Ka*UreE at protein concentrations ≥ 25 μM [35]. The data for the latter protein were interpreted as indicating an initial binding of two Ni^{2+} or Cu^{2+} ions, one after the other, to the interface of the H144**Ka*UreE dimer of dimers, assumed to be the most abundant species in solution. This binding site was suggested to give rise to a tetrameric structure and to involve the four conserved His^{96} residues (one per each monomer) [35]. In the case of *Hp*UreE, however, no oligomerization events occur for the H152A mutant in the presence of Zn^{2+} or Ni^{2+} as demonstrated using light scattering experiments (see Figure S4).

The *Hp*UreE-*Hp*UreG interaction

The available experimental evidences indicate that UreE and UreG form a functional complex in vivo [19, 23, 24]. In order to observe and characterize this interaction in vitro, a solution containing equimolar amounts of the two purified apo-proteins was analyzed by size exclusion chromatography and light scattering (Figure 4A). The result of this experiment indicates that the dimeric *Hp*UreE elutes as a species separated from *Hp*UreG, the latter being present in the monomeric state, as recently reported [16]. Considering that the experimental setup used for the SEC-MALS-QELS measurement represents non-equilibrium conditions, we monitored this interaction more quantitatively using ITC. When a solution of *Hp*UreG was titrated with a solution of *Hp*UreE in the same buffer, clear exothermic peaks were observed (Figure S5A) which, after integration, revealed a curve (Figure 4B) that could be fitted using a single binding event model. The stoichiometry of the interaction suggests that two monomers of *Hp*UreG bind to a single dimer of *Hp*UreE, forming a *Hp*UreE-*Hp*UreG complex having a dissociation constant $K_d = 4.0 \pm 0.3$ μM, $\Delta H = -12.5 \pm 0.9$ kcal mol^{-1}, and $\Delta S = -17.5$ cal mol^{-1} K^{-1}.

Figure 4 here

The formation of the *Hp*UreE-*Hp*UreG complex was also monitored using NMR spectroscopy. The TROSY-HSQC spectrum of the solution containing one equivalent of ^{15}N-*Hp*UreE dimer and two equivalents of unlabeled *Hp*UreG monomer differs from that of *Hp*UreE in the absence of *Hp*UreG (Figure S6A). A general broadening of the peaks is observed, while a number of them experience small chemical shift changes ($\Delta\delta_{av} \leq 0.1$ ppm) consistent with the formation of a complex between the two proteins, as observed by ITC. The number of Gly resonances does not increase upon complex formation, suggesting maintenance of the UreE homodimeric symmetry. Addition of one equivalent of unlabeled *Hp*UreE dimer to a solution of ^{15}N-*Hp*UreG causes broadening beyond detection for most of the backbone amide signals observed in a regular ^{1}H-^{15}N HSQC spectrum (not shown) as compared to

THIS IS NOT THE VERSION OF RECORD - see doi:10.1042/BJ20090434

Accepted Manuscript

Licenced copy. Copying is not permitted, except with prior permission and as allowed by law.
© 2009 The Authors Journal compilation © 2009 Portland Press Limited

the same spectrum of *Hp*UreG [16]. Resonances could be recovered by recording a ^{1}H-^{15}N TROSY-HSQC spectrum (Figure S6B), an effect that can be explained with the large molecular mass (ca. 80 kDa) of the *Hp*UreE-*Hp*UreG complex. Small chemical shift changes on selected resonances of backbone amides are observed ($\Delta\delta_{av} \leq 0.05$ ppm) upon complex formation. An assignment of the resonances, beyond the scope of the present study, would provide information on the surface contact areas, and is currently underway in our laboratories.

The observed 1:2 stoichiometry of the *Hp*UreE-*Hp*UreG complex, coupled to the previously reported dimerization of *Hp*UreG selectively induced by the binding of one equivalent of Zn^{2+} per protein dimer, and not by Ni^{2+}-binding [16], prompted us to explore the role of these two metal ions in the stabilization of the protein complex. The SEC elution profile and molar masses of a mixture of *Hp*UreE and *Hp*UreG in a 1:2 ratio, as measured by MALS, were not affected by the presence of Ni^{2+}, indicating that this metal ion is not capable of significantly stabilizing the protein complex. This is consistent with the absence of a role for Ni^{2+} in the dimerization of *Hp*UreG [16]. On the other hand, when the same experiment was carried out using Zn^{2+}, the elution peaks corresponding to the separate *Hp*UreE and *Hp*UreG proteins completely disappeared, while a new unique peak, with M = 79.4 ± 2 kDa and R_h = 5.8 ± 0.1 nm, was concomitantly observed (Figure 4A). This result indicates that the interaction between *Hp*UreE and *Hp*UreG, leading to the establishment of a complex, is specifically stabilized by Zn^{2+}. On the basis of the theoretical masses of the *Hp*UreE dimer (39 kDa) and of the *Hp*UreG monomer (22 kDa), the mass of the new species formed in the presence of Zn^{2+} is fully consistent with the 1:2 stoichiometry established by ITC.

The molecular model of the *Hp*UreE-*Hp*UreG complex

The viability of the *Hp*UreE-*Hp*UreG complex formation was investigated from a structural modelling point of view. The model structure of the *Hp*UreE dimer was docked onto the model of the dimeric form of *Hp*UreG [16], with optimization of protein backbone and side chains at the interface between the two homodimers. In the resulting structure (Figure 5A,B), the two proteins face each other along their extended axes, and only limited modifications of the proteins backbone, restricted both in extent and in topology distribution, were necessary in order to optimize the docking procedure (Figure 5A). The central pocket formed on the *Hp*UreG surface around the conserved Cys^{66} and His^{68} residues matches the shape and volume of the protruding region around the pair of conserved His^{102} residues on the surface of *Hp*UreE. The shallow crevice formed between the central C-terminal domain and the peripheral N-terminal domain of *Hp*UreE is filled with the bulge found on the surface of *Hp*UreG around the rim of the protein dimerization interface (Figure 5A,B). Overall, a full size, shape, and electric charge complementarity between the surfaces of the two proteins is observed (Figure 5C,D), with the formation of the complex resulting in a large total area (6378 $Å^2$, 40.4% of *Hp*UreE and 36.3% of *Hp*UreG) that is buried by the two interacting homodimers. The details of the interaction are given as Supplementary Information.

Figure 5 here

The role of Zn^{2+} in the stabilization of the *Hp*UreE-*Hp*UreG complex

A recent article has established the key importance of the surface exposed conserved Cys^{66} and His^{68} residues in *Hp*UreG for the binding of Zn^{2+} [16]. Moreover, the present study indicates a role for His^{102} and His^{152} in metal ion binding to *Hp*UreE. The structure of the *Hp*UreE-*Hp*UreG complex features Cys^{66}, His^{68} of *Hp*UreG, and His^{102} of *Hp*UreE, in neighbouring positions in the central region of the complex. This suggests the building up of a novel metal binding site at the interface between the two protein partners (see close-up in Figure 5A). The position of His^{152} cannot be predicted by the model because of the absence of structural data for the terminal disordered region. In order to experimentally verify the presence of this site, we carried out calorimetric titrations of Zn^{2+} onto a solution containing a preformed complex obtained in situ by mixing the two proteins with a 1:2 stoichiometry *Hp*UreE dimer:*Hp*UreG monomer (Figure S5 and 4C). The curve obtained using the wild type proteins reveals indeed an event of binding, characterized by K_d = 1.5 ± 0.3 nM, which is ca. 2-3 orders of magnitude tighter than those observed for isolated *Hp*UreE (this work) or *Hp*UreG [16]. This event is distinct from an additional following binding step with K_d = 0.67 ± 0.05 μM. Therefore,

THIS IS NOT THE VERSION OF RECORD - see doi:10.1042/BJ20090434

Accepted Manuscript

Licenced copy. Copying is not permitted, except with prior permission and as allowed by law.
© 2009 The Authors Journal compilation © 2009 Portland Press Limited

the *Hp*UreE-*Hp*UreG complex binds two Zn^{2+} ions, in a high-affinity and a low-affinity site.

The identity of the residues involved in these two binding events was investigated by repeating the same experiment using, instead of the wild type proteins, the mutants H102K *Hp*UreE, H152A *Hp*UreE, or C66A/H68A *Hp*UreG [16] (Figure 4C). In the case of each of the *Hp*UreE mutants, the tight binding event is not observed, while it is maintained when the mutant of *Hp*UreG is used. On the other hand, the low affinity site is still present when the two mutants of *Hp*UreE are utilized, but is disrupted in the case of C66A/H68A *Hp*UreG. The residual binding of two Zn^{2+} ions in the latter case reproduces what previously observed for the *Hp*UreG double mutant alone [16]. Overall, these data suggest that His^{102} and His^{152} contribute to the building of the high affinity site in the complex, while *Hp*UreG Cys^{66} and His^{68} residues are responsible for the low affinity binding event. The exact topology of these two metal binding sites cannot be determined at the present stage of the study given the limited structural information on the flexible C-terminal pendant arms containing His^{152}. However, the calculated model structure of the protein complex allows us to speculate that these protein regions could adapt their conformation to fill the cleft that is formed between the proteins interaction surfaces (Figure 5B), bringing His^{152} close to the metal binding site that also involves His^{102}. On the other hand, the lower affinity binding event could involve a nearby site situated close to Cys^{66} and His^{68} on *Hp*UreG. It is worth mentioning here that crystallographic evidence indicates the presence of a dinuclear Zn^{2+} binding site on the surface of *Mj*HypB (a close homologue to *Hp*UreG), which involves a Cys and a His residue corresponding to Cys^{66} and His^{68} on *Hp*UreG [31].

The stabilization of a *Hp*UreE-*Hp*UreG complex in the presence of Zn^{2+} is significant within the framework of the known role of *Hp*UreG in vivo: this protein is an enzyme that catalyzes GTP hydrolysis necessary to the urease activation process [10]. *Hp*UreG belongs to a class of homo-dimeric GTPases (or ATPases) that use GTP (or ATP) hydrolysis as a conserved molecular switch to regulate a large number of cellular processes [44]. The activity of these hydrolases is, in general, tightly controlled by different factors, such as protein dimerization and subsequent interaction with GAP (GTPase activator protein) and GEF (guanine nucleotide exchange factor) proteins. These GTPase regulators are stable functional dimers, as observed for UreE. In order to test a possible role for *Hp*UreE in modulating the enzymatic cycle of *Hp*UreG, we measured the GTPase activity of the *Hp*UreE-*Hp*UreG complex formed in the presence of Zn^{2+} using both a colorimetric and an enzymatic method, as previously described [16]. We found that the interaction with *Hp*UreE stabilized by Zn^{2+} is not sufficient to promote any detectable GTPase activity. This result is not surprising: it is known that the GTP-dependent process of nickel incorporation into apo-urease occurs only in the presence of a UreDFG complex, implying that UreD and UreF must also play an essential role in UreG activation.

Conclusions

The results presented here allow us to envisage a mechanism for the urease assembly that entails a specific role for both Ni^{2+} and Zn^{2+} ions. An exchange of Zn^{2+} for Ni^{2+} binding to *Hp*UreE could be the initial switch that modulates the interaction between *Hp*UreE and *Hp*UreG. Ni^{2+} released from *Hp*UreE could be incorporated into the apo-urease active site, concomitantly with the Zn^{2+}-induced *Hp*UreE-*Hp*UreG complex formation and consequent stimulation of GTPase activity catalyzed by *Hp*UreG. This step would lead to the carbamylation of the lysine residue in the urease active site, thus finalizing the activation of the enzyme.

The chaperones involved in the maturation of [NiFe]-hydrogenase in *E. coli*, like HypA (and its homologue HybF) [38, 45] and HypB [46], also display a specific Zn^{2+}-binding capability. On the other hand, HypA from *H. pylori*, responsible for the activation of both urease and hydrogenase enzymes [47], shows Ni^{2+}-binding capability in vitro [48]. The occurrence of a specific interaction between dimeric HypA and UreE from *H. pylori* was proved using cross-linking and immuno-blotting experiments, suggesting that this interaction is functional to mediate Ni^{2+} transfer from HypA to UreE in vivo [49]. Specific protein-protein interactions were observed between HypA and HypB during cross-linking experiments, as well as between HypB and UreG from tandem affinity purification [50]. These data, coupled to the observation of specific UreE-UreG interactions, indicate the possible presence of cross-talk mechanisms in vivo, involving HypA, HypB, UreG and UreE. It is interesting to notice that all these proteins possess Ni^{2+} and/or Zn^{2+} binding capability. Therefore, the Zn^{2+}-dependent interaction between *Hp*UreE and *Hp*UreG, as well as the interdependence between Ni^{2+} and

THIS IS NOT THE VERSION OF RECORD - see doi:10.1042/BJ20090434

Accepted Manuscript

Licenced copy. Copying is not permitted, except with prior permission and as allowed by law.
© 2009 The Authors Journal compilation © 2009 Portland Press Limited

Zn^{2+}, emerging in this study for the *H. pylori* urease system, suggests a functional role for metal binding to these accessory proteins, modulating the formation of the protein-protein complexes necessary for enzyme maturation. These observations represent a paradigmatic general point to understand the role of Zn^{2+} in the process of Ni^{2+} delivery and incorporation in different enzymes.

FUNDING
Work supported by MIUR-PRIN2007. The VP-ITC instrument is property of CIRB-UniBO. The fellowships for MB and FM are provided by UniBO. BZ was supported by Consorzio Interuniversitario di Risonanze Magnetiche di Metalloproteine Paramagnetiche and by UniBO.

REFERENCES

1 Bruce, M. G. and Maaroos, H. I. (2008) Epidemiology of *Helicobacter pylori* infection. Helicobacter. **13 Suppl 1**, 1-6

2 Ferreira, A. C., Isomoto, H., Moriyama, M., Fujioka, T., Machado, J. C. and Yamaoka, Y. (2008) *Helicobacter* and gastric malignancies. Helicobacter. **13 Suppl 1**, 28-34

3 Callahan, B. P., Yuan, Y. and Wolfenden, R. (2005) The burden borne by urease. J. Am. Chem. Soc. **127**, 10828-10829

4 Dixon, N. E., Gazzola, C., Blakeley, R. and Zerner, B. (1975) Jack bean urease (EC 3.5.1.5). A metalloenzyme. A simple biological role for nickel? J. Am. Chem. Soc. **97**, 4131-4132

5 Jabri, E., Carr, M. B., Hausinger, R. P. and Karplus, P. A. (1995) The crystal structure of urease from *Klebsiella aerogenes*. Science. **268**, 998-1004

6 Benini, S., Rypniewski, W. R., Wilson, K. S., Miletti, S., Ciurli, S. and Mangani, S. (1999) A new proposal for urease mechanism based on the crystal structures of the native and inhibited enzyme from *Bacillus pasteurii*: why urea hydrolysis costs two nickels. Structure. **7**, 205-216

7 Ha, N.-C., Oh, S.-T., Sung, J. Y., Cha, K. A., Lee, M. H. and Oh, B.-H. (2001) Supramolecular assembly and acid resistance of *Helicobacter pylori* urease. Nat. Struct. Biol. **8**, 505-509

8 Sheridan, L., Wilmot, C. M., Cromie, K. D., van der Logt, P. and Phillips, S. E. V. (2002) Crystallization and preliminary X-ray structure determination of jack bean urease with a bound antibody fragment. Acta Cryst. D. **58**, 374-376

9 Ciurli, S. (2007) Urease. Recent insights in the role of nickel. In Nickel and its surprising impact in nature. pp. 241-278, John Wiley & Sons, Ltd., Chichester, UK

10 Quiroz, S., Kim, J. K., Mulrooney, S. B. and Hausinger, R. P. (2007) Chaperones of nickel metabolism. In Nickel and its surprising impact in nature. pp. 519-544, John Wiley & Sons, Ltd., Chichester, UK

11 Park, I.-S. and Hausinger, R. P. (1996) Metal ion interactions with urease and UreD-urease apoproteins. Biochemistry. **35**, 5345-5352

12 Quiroz-Valenzuela, S., Sukuru, S. C., Hausinger, R. P., Kuhn, L. A. and Heller, W. T. (2008) The structure of urease activation complexes examined by flexibility analysis, mutagenesis, and small-angle X-ray scattering. Arch. Biochem. Biophys. **480**, 51-57

13 Zambelli, B., Stola, M., Musiani, F., De Vriendt, K., Samyn, B., Devreese, B., Van Beeumen, J., Turano, P., Dikiy, A., Bryant, D. A. and Ciurli, S. (2005) UreG, a chaperone in the urease assembly process, is an intrinsically unstructured GTPase that specifically binds Zn^{2+}. J. Biol. Chem. **280**, 4684-4695

14 Neyroz, P., Zambelli, B. and Ciurli, S. (2006) Intrinsically disordered structure of *Bacillus pasteurii* UreG as revealed by steady-state and time-resolved fluorescence spectroscopy. Biochemistry. **45**, 8918-8930

15 Zambelli, B., Musiani, F., Savini, M., Tucker, P. and Ciurli, S. (2007) Biochemical studies on *Mycobacterium tuberculosis* UreG and comparative modeling reveal structural and functional conservation among the bacterial UreG family. Biochemistry. **46**, 3171-3182

16 Zambelli, B., Turano, P., Musiani, F., Neyroz, P. and Ciurli, S. (2009) Zn^{2+}-linked dimerization of UreG from *Helicobacter pylori*, a metallo-chaperone involved in nickel trafficking and urease activation. Proteins: Struct. Funct. and Bioinform. **74**, 222-239

THIS IS NOT THE VERSION OF RECORD - see doi:10.1042/BJ20090434

Accepted Manuscript

Licenced copy. Copying is not permitted, except with prior permission and as allowed by law.
© 2009 The Authors Journal compilation © 2009 Portland Press Limited

17 Salomone-Stagni, M., Zambelli, B., Musiani, F. and Ciurli, S. (2007) A model-based proposal for the role of UreF as a GTPase-activating protein in the urease active site biosynthesis. Proteins: Struct. Funct. and Bioinform. **68**, 749-761

18 Park, I. S. and Hausinger, R. P. (1995) Requirement of carbon dioxide for in vitro assembly of the urease nickel metallocenter. Science. **267**, 1156-1158

19 Soriano, A., Colpas, G. J. and Hausinger, R. P. (2000) UreE stimulation of GTP-dependent urease activation in the UreD-UreF-UreG-urease apoprotein complex. Biochemistry. **39**, 12435-12440

20 Remaut, H., Safarov, N., Ciurli, S. and Van Beeumen, J. (2001) Structural basis for Ni^{2+} transport and assembly of the urease active site by the metallochaperone UreE from *Bacillus pasteurii*. J. Biol. Chem. **276**, 49365-49370

21 Song, H.-K., Mulrooney, S. B., Huber, R. and Hausinger, R. P. (2001) Crystal structure of *Klebsiella aerogenes* UreE, a nickel-binding metallochaperone for urease activation. J. Biol. Chem. **276**, 49359-49364

22 Musiani, F., Zambelli, B., Stola, M. and Ciurli, S. (2004) Nickel trafficking: insights into the fold and function of UreE, a urease metallochaperone. J. Inorg. Biochem. **98**, 803-813

23 Rain, J. C., Selig, L., De Reuse, H., Battaglia, V., Reverdy, C., Simon, S., Lenzen, G., Petel, F., Wojcik, J., Schachter, V., Chemama, Y., Labigne, A. and Legrain, P. (2001) The protein-protein interaction map of *Helicobacter pylori*. Nature. **409**, 211-215

24 Voland, P., Weeks, D. L., Marcus, E. A., Prinz, C., Sachs, G. and Scott, D. (2003) Interactions among the seven *Helicobacter pylori* proteins encoded by the urease gene cluster. Am. J. Physiol. Gastrointest. Liver Physiol. **284**, G96-G106

25 Benoit, S. and Maier, R. J. (2003) Dependence of *Helicobacter pylori* urease activity on the nickel-sequestering ability of the UreE accessory protein. J. Bacteriol. **185**, 4787-4795

26 Sklenar, V., Piotto, M., Leppik, R. and Saudek, V. (1993) Gradient-tailored water suppression for ^{1}H-^{15}N HSQC experiments optimized to retain full sensitivity. J. Magn. Reson., Ser. A. **102**, 241-245

27 Pervushin, K., Riek, R., Wider, G. and Wuthrich, K. (1997) Attenuated T_2 relaxation by mutual cancellation of dipole-dipole coupling and chemical shift anisotropy indicates an avenue to NMR structures of very large biological macromolecules in solution. Proc. Natl. Acad. Sci. USA. **94**, 12366-12371.

28 Charlwood, P. A. (1957) Partial specific volumes of proteins in relation to composition and environment. J. Am. Chem. Soc. **79**, 776-781

29 Marti-Renom, M. A., Stuart, A. C., Fiser, A., Sanchez, R., Melo, F. and Sali, A. (2000) Comparative protein structure modeling of genes and genomes. Annu. Rev. Biophys. Biomol. Struct. **29**, 291-325

30 Gray, J. J., Moughon, S., Wang, C., Schueler-Furman, O., Kuhlman, B., Rohl, C. A. and Baker, D. (2003) Protein-protein docking with simultaneous optimization of rigid-body displacement and side-chain conformations. J. Mol. Biol. **331**, 281-299

31 Gasper, R., Scrima, A. and Wittinghofer, A. (2006) Structural insights into HypB, a GTP-binding protein that regulates metal binding. J. Biol. Chem. **281**, 27492-27502

32 Cuff, J. A., Clamp, M. E., Siddiqui, A. S., Finlay, M. and Barton, G. J. (1998) Jpred: A Consensus Secondary Structure Prediction Server. Bioinformatics. **14**, 892-893

33 Kabsch, W. and Sander, C. (1983) Dictionary of protein secondary structure; pattern recognition of hydrogen-bonded and geometrical features. Biopolymers. **22**, 2577-2637

34 Won, H. S., Lee, Y. H., Kim, J. H., Shin, I. S., Lee, M. H. and Lee, B. J. (2004) Structural characterization of the nickel-binding properties of *Bacillus pasteurii* urease accessory protein (Ure)E in solution. J. Biol. Chem. **279**, 17466-17472

35 Grossoehme, N. E., Mulrooney, S. B., Hausinger, R. P. and Wilcox, D. E. (2007) Thermodynamics of Ni^{2+}, Cu^{2+}, and Zn^{2+} binding to the urease metallochaperone UreE. Biochemistry. **46**, 10506-10516

36 Ciurli, S., Safarov, N., Miletti, S., Dikiy, A., Christensen, S. K., Kornetzky, K., Bryant, D. A., Vandenberghe, I., Devreese, B., Samyn, B., Remaut, H. and van Beeumen, J. (2002) Molecular characterization of *Bacillus pasteurii* UreE, a metal-binding chaperone for the assembly of the urease

THIS IS NOT THE VERSION OF RECORD - see doi:10.1042/BJ20090434

Accepted Manuscript

Licenced copy. Copying is not permitted, except with prior permission and as allowed by law.
© 2009 The Authors Journal compilation © 2009 Portland Press Limited

active site. J. Biol. Inorg. Chem. **7**, 623-631
37 Blokesch, M., Rohrmoser, M., Rode, S. and Bock, A. (2004) HybF, a zinc-containing protein involved in NiFe hydrogenase maturation. J. Bacteriol. **186**, 2603-2611
38 Atanassova, A. and Zamble, D. B. (2005) *Escherichia coli* HypA is a zinc metalloprotein with a weak affinity for nickel. J. Bacteriol. **187**, 4689-4697
39 Stola, M., Musiani, F., Mangani, S., Turano, P., Safarov, N., Zambelli, B. and Ciurli, S. (2006) The nickel site of *Bacillus pasteurii* UreE, a urease metallo-chaperone, as revealed by metal-binding studies and X-ray absorption spectroscopy. Biochemistry. **45**, 6495-6509
40 Kennedy, D. C., Herbst, R. W., Iwig, J. S., Chivers, P. T. and Maroney, M. J. (2007) A dynamic Zn site in *Helicobacter pylori* HypA: a potential mechanism for metal-specific protein activity. J. Am. Chem. Soc. **129**, 16-17
41 Brayman, T. G. and Hausinger, R. P. (1996) Purification, characterization, and functional analysis of a truncated *Klebsiella aerogenes* UreE urease accessory protein lacking the histidine-rich carboxyl terminus. J. Bacteriol. **178**, 5410-5416
42 Colpas, G. J., Brayman, T. G., Ming, L. J. and Hausinger, R. P. (1999) Identification of metal-binding residues in the *Klebsiella aerogenes* urease nickel metallochaperone, UreE. Biochemistry. **38**, 4078-4088
43 Mulrooney, S. B. and Hausinger, R. P. (2003) Nickel uptake and utilization by microorganisms. FEMS Microbiol. Rev. **27**, 239-261
44 Leipe, D. D., Wolf, Y. I., Koonin, E. V. and Aravind, L. (2002) Classification and evolution of P-loop GTPases and related ATPases. J. Mol. Biol. **317**, 41-72
45 Blokesch, M., Rohrmoser, M., Rode, S. and Bock, A. (2004) HybF, a zinc-containing protein involved in NiFe hydrogenase maturation. J. Bacteriol. **186**, 2603-2611
46 Leach, M. R., Sandal, S., Sun, H. and Zamble, D. B. (2005) Metal binding activity of the *Escherichia coli* hydrogenase maturation factor HypB. Biochemistry. **44**, 12229-12238
47 Olson, J. W., Mehta, N. S. and Maier, R. J. (2001) Requirement of nickel metabolism proteins HypA and HypB for full activity of both hydrogenase and urease in *Helicobacter pylori*. Mol. Microbiol. **39**, 176-182
48 Mehta, N., Olson, J. W. and Maier, R. J. (2003) Characterization of *Helicobacter pylori* nickel metabolism accessory proteins needed for maturation of both urease and hydrogenase. J. Bacteriol. **185**, 726-734
49 Benoit, S. L., Mehta, N., Weinberg, M. V., Maier, C. and Maier, R. J. (2007) Interaction between the *Helicobacter pylori* accessory proteins HypA and UreE is needed for urease maturation. Microbiology. **153**, 1474-1482
50 Stingl, K., Schauer, K., Ecobichon, C., Labigne, A., Lenormand, P., Rousselle, J. C., Namane, A. and de Reuse, H. (2008) In vivo interactome of *Helicobacter pylori* urease revealed by tandem affinity purification. Mol. Cell. Proteomics

THIS IS NOT THE VERSION OF RECORD - see doi:10.1042/BJ20090434

Accepted Manuscript

Licenced copy. Copying is not permitted, except with prior permission and as allowed by law.
© 2009 The Authors Journal compilation © 2009 Portland Press Limited

THIS IS NOT THE VERSION OF RECORD - see doi:10.1042/BJ20090434

Accepted Manuscript

FIGURE LEGENDS

Figure 1. Structural comparison and sequence alignment of *Hp*UreE, *Bp*UreE and *Ka*UreE. **A**. Crystal structures of *Bp*UreE (PDB code 1EAR) and H144**Ka*UreE (PDB code 1GMW), shown as ribbon diagrams. Histidine residues involved in metal binding sites, and the corresponding non-conserved residues, are shown as ball-and-stick. **B.** Sequence alignment of *Hp*UreE, *Bp*UreE, and *Ka*UreE; the secondary structure elements are highlighted in boxes (helices) and light gray(sheets). The C-terminal His-rich tail of *Ka*UreE is italics and underlined. Histidine residues, representing the conserved and non-conserved nickel-binding sites, are bold-faced.

Figure 2. CD, NMR, and MALS/QELS of *Hp*UreE. A. Far-UV circular dichroism spectrum of *Hp*UreE. The experimental data are shown as dots. The solid line represents the best fit calculated for apo-*Hp*UreE using the CDSSTR program available at the Dichroweb server. Mean residue ellipticity units are degrees cm^2 $dmol^{-1}$ $residue^{-1}$. **B.** ^1H-^{15}N TROSY-HSQC spectrum of 200 μM apo-*Hp*UreE, acquired at 800 MHz and 298 K. **C** Plot of the molar mass distribution for *Hp*UreE. The solid lines indicate the Superdex S-200 size-exclusion elution profile monitored by the refractive index detector, and the symbols are the weight-averaged molecular masses for each slice, measured every second. Data obtained in the absence of metal ions (thin line, filled dots) and in the presence of Ni^{2+} (thick line, hollow circles) or Zn^{2+} (line, hollow squares) are reported. The average molecular mass and the hydrodynamic radius of apo-*Hp*UreE are indicated.

Figure 3. ITC data of $NiSO_4$ and $ZnSO_4$ binding to wild type *Hp*UreE and its H102 K and H152A mutants. Representative plots of titration data showing the thermal effect of 30 x 10 μL injections of Ni^{2+} (100 μM) (panel **A**) and Zn^{2+} (100 μM) (panel **B**) respectively, onto a solution of wild type *Hp*UreE (10 μM), together with the best fits of the integrated data, represented as solid lines, obtained by a non-linear least squares procedure. The calculated numbers of sites and dissociation constants are indicated. The corresponding experiments performed using the H102K *Hp*UreE mutant are shown as hollow circles. In panels **C** and **D** the data and fits obtained using the H152A *Hp*UreE mutant, in the same experimental conditions, are shown.

Figure 4. *Hp*UreE-*Hp*UreG interaction analysis. **A**. The solid lines indicate the Superdex S-200 size-exclusion elution profile monitored by the refractive index detector of a solution containing *Hp*UreE (one equivalent of dimer) and *Hp*UreG (two equivalents of monomer), in the absence (thin line) or in the presence (thick line) of two equivalents of Zn^{2+}. Data of apo-*Hp*UreE and apo-*Hp*UreG (dashed lines) are shown as references. The dots are the weight-averaged molecular masses for each slice, measured every second. **B.** Best fit of the integrated raw ITC data of the titration of 50 μM *Hp*UreG monomer with 160 μM *Hp*UreE dimer, represented as a solid line, obtained by a non-linear least squares procedure. The calculated values for the stoichiometry and dissociation constant are indicated. **C**. Best fit of the integrated raw ITC data of the titration of 5 μM *Hp*UreE-*Hp*UreG complex, and its related mutants, with 70 μM $ZnSO_4$, represented as a solid line, obtained by a non-linear least squares procedure (wild type: filled circles; H102K *Hp*UreE - *Hp*UreG: filled squares; H152A *Hp*UreE - *Hp*UreG: hollow squares; *Hp*UreE - C66A/H68A *Hp*UreG: hollow circles). The calculated values for the dissociation constant for the wild type complex are indicated. The calorimetric parameters derived from all fits are given in Table S2.

Figure 5. Model of the *Hp*UreE-*Hp*UreG interaction. Ribbon diagram (**A**) and solvent excluded surface (**B**) of the model structure of the *Hp*UreE-*Hp*UreG complex (*Hp*UreE *orange*, *Hp*UreG *light blue*). In the right side of panel **A** the ribbons are coloured according to the backbone root mean square deviation with respect to the separated protein model structures, ranging from 0.0 Å (*green*) to 0.75 Å (*yellow*) to greater than 1.5 Å (*red*). Residues found at the interface of the complex and known to be involved in metal binding (*Hp*UreE His^{102} and *Hp*UreG Cys^{66} and His^{68}) are shown as ball and stick models. In panels **A** and **B,** the positions of two GTPγS molecules and the nearby Mg^{2+} ions are shown. The position of the surface clefts are indicated in panel **B**. Atom colour scheme: Mg, *dark green*; C, *grey*; H, *white*; N, *blue*; and O, *red*. Panels **C** and **D** report the solvent excluded surfaces of two components of the *Hp*UreE-*Hp*UreG complex oriented in order to expose the interaction surfaces. In panel **C** the surface is coloured according to the distance between the docked proteins: *gray*: > 10 Å; *red*: 5 - 10 Å; *yellow*: 2.5 – 5 Å; *green*: < 2.5 Å. In panel **D** the surface is coloured according to the surface electrostatic potential.

Licenced copy. Copying is not permitted, except with prior permission and as allowed by law.
© 2009 The Authors Journal compilation © 2009 Portland Press Limited

Figure 1

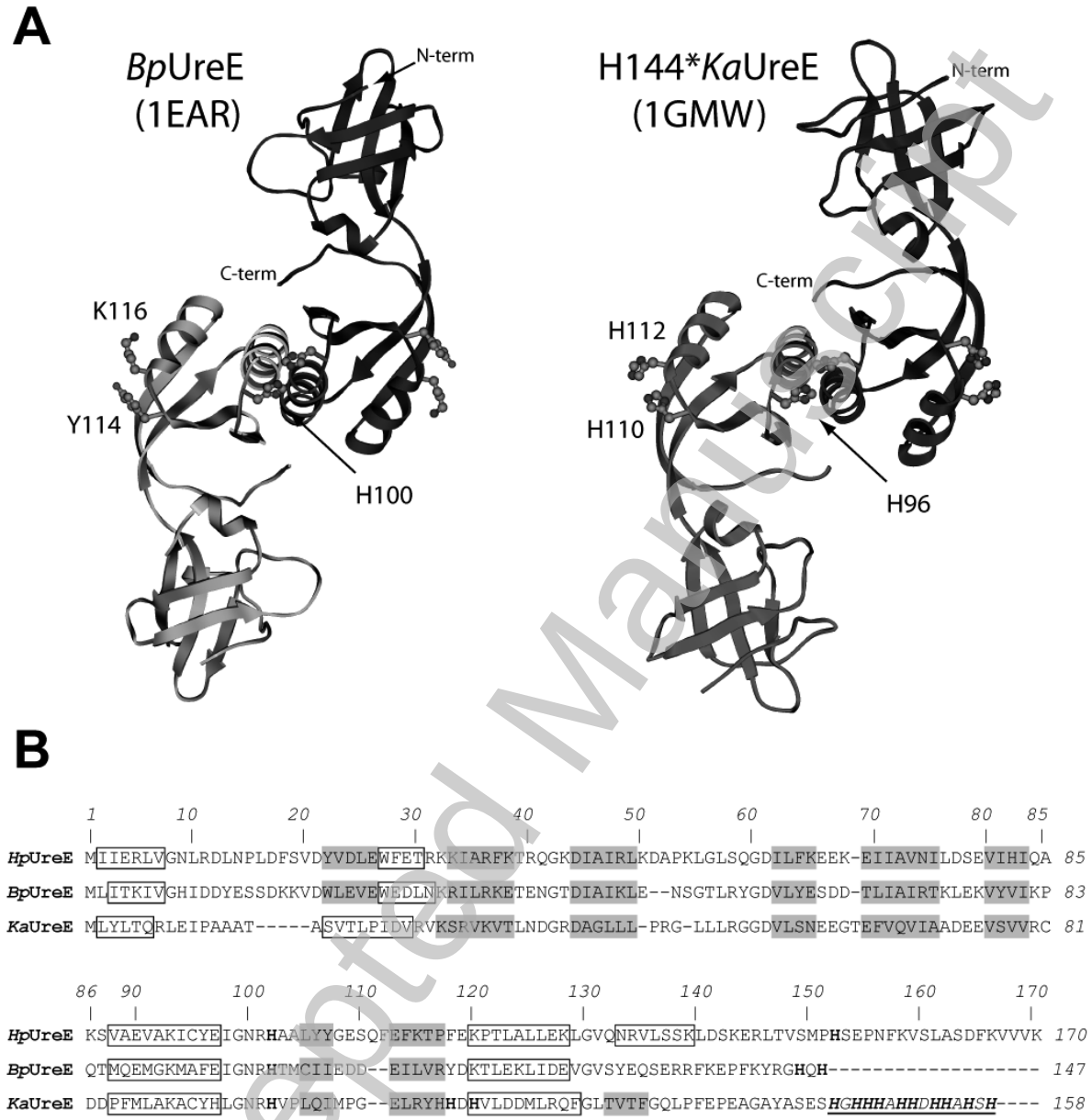

THIS IS NOT THE VERSION OF RECORD - see doi:10.1042/BJ20090434

Accepted Manuscript

Licenced copy. Copying is not permitted, except with prior permission and as allowed by law.
© 2009 The Authors Journal compilation © 2009 Portland Press Limited

Figure 2

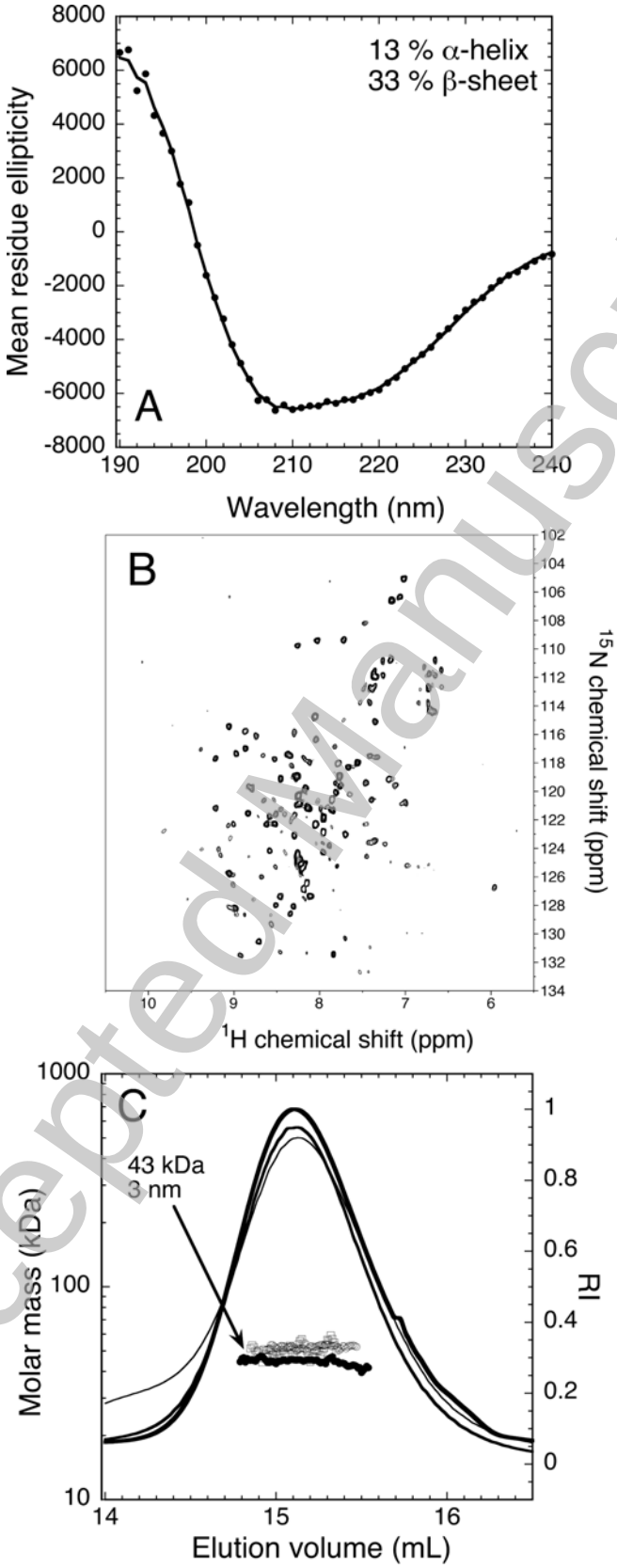

THIS IS NOT THE VERSION OF RECORD - see doi:10.1042/BJ20090434

Accepted Manuscript

Licenced copy. Copying is not permitted, except with prior permission and as allowed by law.
© 2009 The Authors Journal compilation © 2009 Portland Press Limited

Figure 3

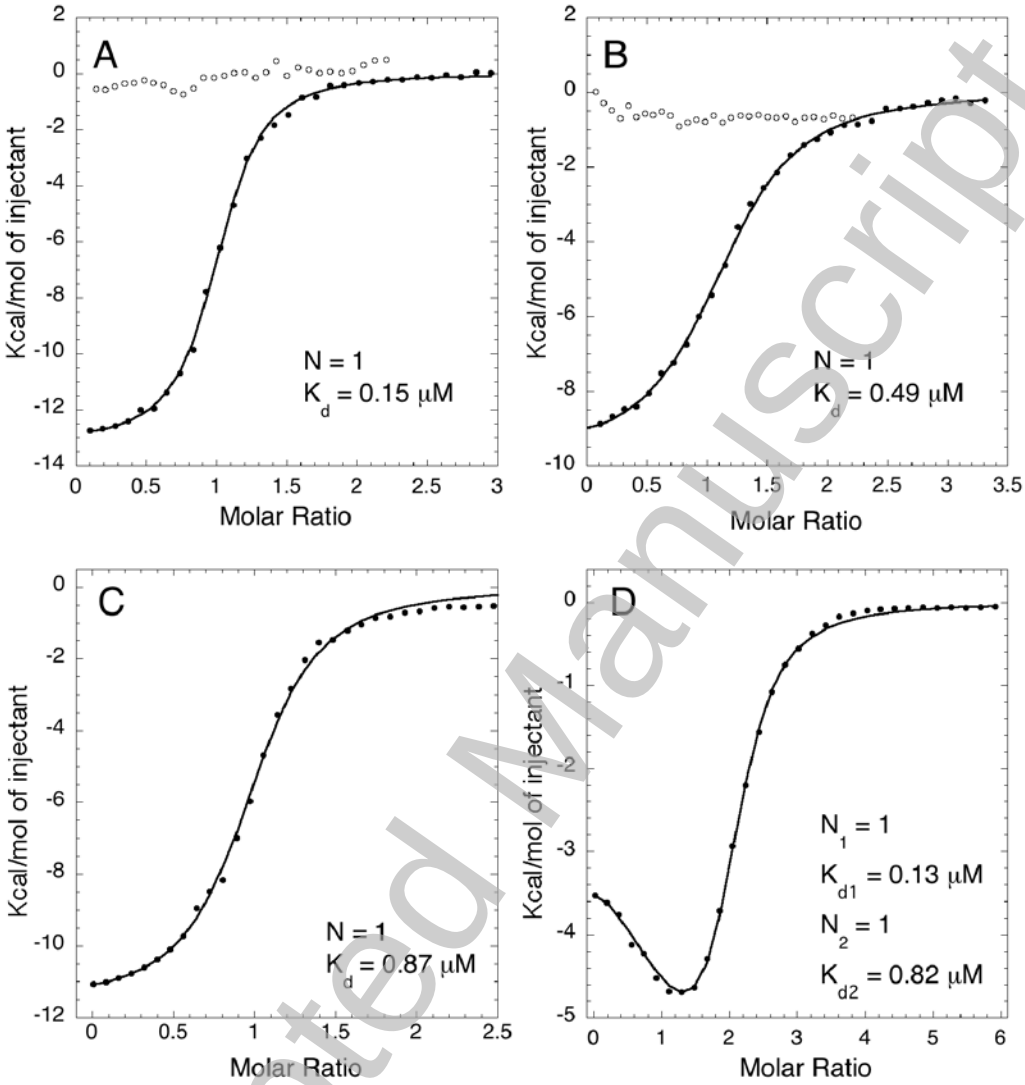

THIS IS NOT THE VERSION OF RECORD - see doi:10.1042/BJ20090434

Accepted Manuscript

Licenced copy. Copying is not permitted, except with prior permission and as allowed by law.
© 2009 The Authors Journal compilation © 2009 Portland Press Limited

Figure 4

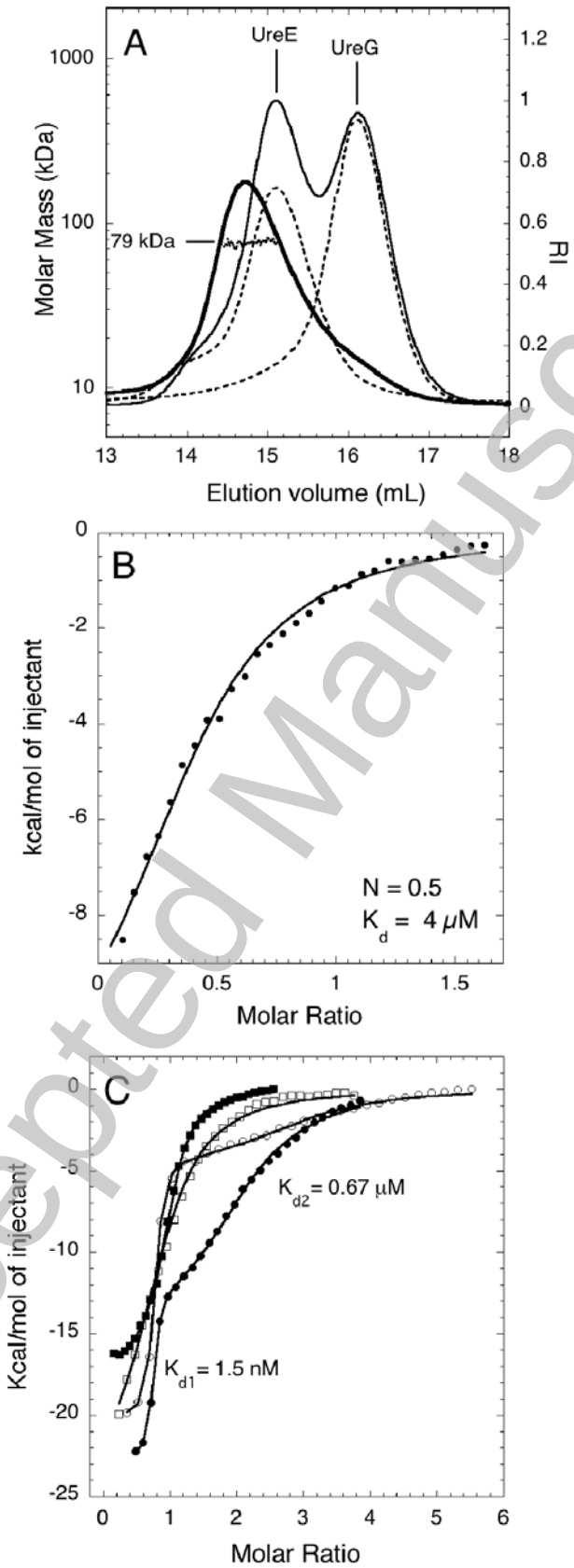

THIS IS NOT THE VERSION OF RECORD - see doi:10.1042/BJ20090434

Accepted Manuscript

Licenced copy. Copying is not permitted, except with prior permission and as allowed by law.
© 2009 The Authors Journal compilation © 2009 Portland Press Limited

Figure 5

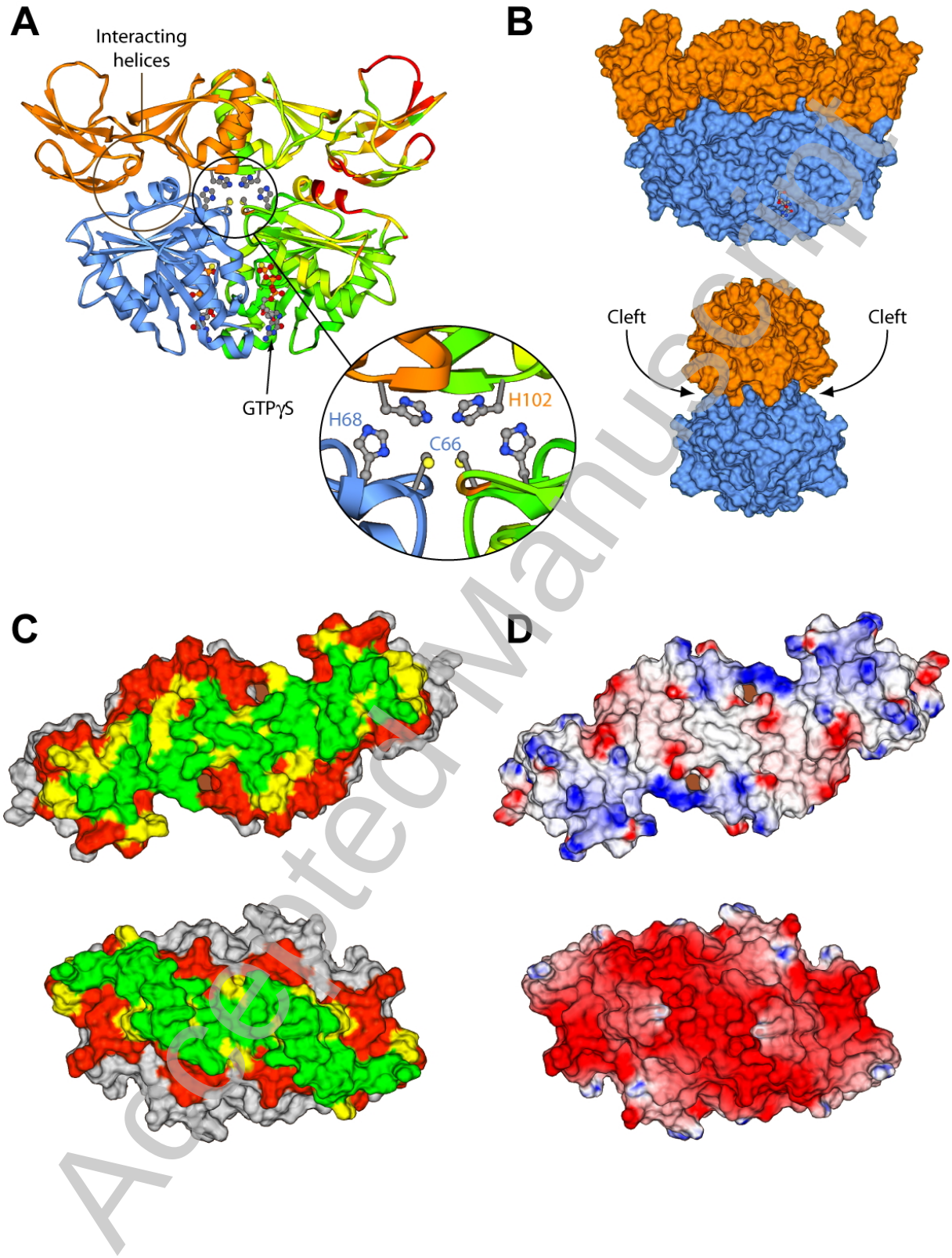

THIS IS NOT THE VERSION OF RECORD - see doi:10.1042/BJ20090434

Accepted Manuscript

Licenced copy. Copying is not permitted, except with prior permission and as allowed by law.
© 2009 The Authors Journal compilation © 2009 Portland Press Limited